JOURNAL OF SOLID STATE CHEMISTRY 76, 345–354 (1988)

Formation and Luminescence of Lower Symmetrical Tellurite Anti-glass Phases

M. TRÖMEL* AND E. MÜNCH

Institut für Anorganische Chemie, Niederurseler Hang, D-6000 Frankfurt 50, Federal Republic of Germany

AND G. BLASSE AND G. J. DIRKSEN

Physical Laboratory, State University, P.O. Box 80.000, 3508 TA Utrecht, The Netherlands

Received September 8, 1987; in revised form April 11, 1988

Two series of nonstoichiometric lanthanoid tellurite phases have been identified which are similar to cubic $(Ln,Te)O_n$ anti-glass phases with CaF_2 defect structure. Their X-ray diagrams indicate low-symmetrical CaF_2 superstructures. Monoclinic (or pseudotetragonal) subcells were determined. Anti-glass disorder is consistent with the Eu^{2+} and Te^{4+} luminescence of one series, but can be excluded for the other one. © 1988 Academic Press, Inc.

Introduction

Anti-glass phases have been described as metal-oxide modified TeO_2 with the fluorite structure, e.g., $SrTe_5O_{11}$ (*1*) and $Ln_2Te_6O_{15}$ (Ln = lanthanoids or Y) (*2*). An anti-glass is here defined as a solid with long-range order, but with highly disturbed short-range order, i.e., varying coordination from one atom to the other which is apparent from the large Debye–Waller parameters (*1, 2*). In a simple glass, e.g., SiO_2 glass, we have the reversed situation. Additionally, in the fluorite-structured tellurite anti-glass the metal ions and Te^{4+} ions are statistically distributed in the cation positions; the anion positions are incompletely occupied.

Recently we have reported on the luminescence of two series of cubic anti-glass tellurites of La, Gd, and Y, one Te-rich and the other Ln-rich (*3*). These are the first examples of oxidic systems containing Te^{4+} ($5s^2$) ions which show luminescence. Metal ions with s^2 configuration are well known for their luminescence (*4*) and have been studied in detail (*5*). It has been shown that the Stokes shift of the emission is related to the amount of space which is available for the s^2 ion in the lattice. Very large Stokes shifts have been observed for s^2 ions in an asymmetrical coordination which is characteristic of these ions. In this respect the well-known $Bi_4Ge_3O_{12}$ has become a famous example (*6*).

The normal fluorite lattice does not meet the geometrical requirements of the Te^{4+}

* To whom correspondence should be addressed.

0022-4596/88 $3.00

coordination in oxides (*7*). However, by large atomic displacements and partly due to the presence of anion vacancies it is possible to provide irregular coordinations. The Te^{4+} luminescence points into the same direction (*3*).

The reported lanthanoid tellurite anti-glass phases are formed at 800–850°C. At higher temperatures, noncubic phases are formed, the structures of which appeared to be derived from the fluorite structure by lowering of symmetry (*8*). If these were anti-glass phases also, not only the number but also the structure types of such phases would be enlarged. The determination of the extremely high Debye–Waller factors, however, which are characteristic of anti-glass disorder requires the complete determination of crystal structure.

In this paper, the lower symmetrical phases have been investigated in two completely different ways, viz., by X-ray diffraction and by luminescence measurements. The former technique reveals long-range order properties, whereas the latter is more suitable to the study of short-range order properties. The Te^{4+} ions show only broadband luminescence spectra which are not very sensitive to change in the Te^{4+} coordination. Therefore we used as one of the lanthanoid ions the Eu^{3+} ion. Its emission spectrum is very sensitive to the nature of its surroundings (*9*).

The two techniques yielded some unexpected results which agree very satisfactorily with Raman–spectroscopical data to be presented elsewhere (*10*).

Experimental

By heating *Ln*-richer cubic anti-glass phases (*2*) or mixtures of TeO_2 (99.9%, Merck) and rare-earth oxides Ln_2O_3, but Pr as Pr_6O_{11} (Sigma, Ventron), for 2 hr up to 3 days under 99.9% N_2 at 900–1050°C, noncubic phases were formed by loss of TeO_2 and small portions of Te. X-ray powder diagrams were taken with a Rigaku SG-9R diffractometer (Cu$K\alpha$ radiation, Ni filter) and, for recording extremely weak reflections, with a Siemens D 500 diffractometer using crystal-monochromatized Cu$K\alpha$ radiation.

Small, but largely varying contents of "active" oxygen (i.e., oxidizing agent) in the samples were determined by the Bunsen method (dissolving in half-concentrated HCl solution, distilling the chlorine into a solution of KI, titration of I_2 by thiosulfate, see (*11*)). The proportion of active oxygen is presented below as Te^{6+}, though it cannot be distinguished from a possible Ln^{4+} content. The overall composition of the samples was calculated from the weight losses during their formation and from the Te^{6+} contents.

The optical measurements were performed in the same way as described in Ref. (*3*).

Results and Discussion

A. X-Ray Diffraction

Two series of noncubic phases were identified and can be distinguished unambiguously for the elements La–Gd from their stronger reflections (Tables 1 and 2). Their compositions (Table 3) were determined from samples, the X-ray diagrams of which showed no reflections of other phases. The accuracy of compositions is low, since phase impurities of about 1% or less can hardly be detected in this way. It is sufficient, however, to recognize a tendency toward lower *Ln*:Te ratios with decreasing ionic radius of *Ln* for the first series, and shifts of lattice constants with composition for two phases in the other one (see Table 3). These changes cannot be explained except by assuming statistical distribution of *Ln* and Te at least in some of the atomic positions.

The first series (*Ln* = Y or La–Ho, but Ce and Tb missing, Pm not investigated)

TABLE I

OBSERVED *d* VALUES FOR FIRST SERIES OF LOWER SYMMETRICAL ANTI-GLASS-RELATED PHASES ("MONOCLINIC I")

h k l	Y	La	Pr	Nd	Sm	Eu	Gd	Dy	Ho
1 1−1	313.4	326.4	321.7	321.0	321.3	317.6	316.3	314.7	313.3
1 1 1	312.7	325.3	320.2	319.4	319.5	316.6	315.0	313.6	312.7
2 0 0	276.6	288.0	283.9	283.4	281.9	279.8	279.0	277.0	276.3
0 0 2	272.3	284.4	280.5	279.6	278.6	276.0	275.2	273.2	272.2
0 2 0	265.0	273.6	271.4	270.1	270.7	267.6	267.3	265.7	264.5
2 0−2	194.4	203.4	200.4	200.1	198.8	197.3	196.7	195.1	194.3
2 0 2	193.5	201.7	199.2	198.3	197.4	195.7	195.0	193.7	193.0
2 2 0	191.2	198.8	196.3	195.6	195.1	193.4	193.1	191.7	191.0
0 2 2	189.7	197.5	195.2	194.5	194.0	192.2	191.7	190.1	189.7
3 1−1	165.8	173.2	170.7	170.5	169.4	168.2	167.7	166.5	165.8
3 1 1	165.6	172.7	170.4	169.7	168.8	167.8	167.0	165.4	165.4
1 1−3	164.1	171.9	169.4	168.8	167.8	166.6	166.2	164.8	164.3
1 1 3	163.7	171.0	168.8	167.8	167.2	166.0	165.5	164.3	163.5
1 3−1	160.7	166.6	164.8	164.5	164.4	162.7	162.6	161.1	160.9
1 3 1	160.7	166.3	164.8	164.1	163.9	162.3	162.2	160.9	160.4
2 2−2	156.7	163.4	161.2	160.9	160.3	158.7	158.4	157.3	156.6
2 2 2	156.1	162.5	160.7	159.9	159.6	158.1	157.4	156.6	155.9
4 0 0	138.1	144.2	142.1	141.9	141.0	140.0	—	138.3	138.0
0 0 4	135.9	142.3	140.4	139.8	—	138.1	137.6	136.5	135.8
0 4 0	132.4	136.8	—	—	—	133.7	133.7	132.5	—
3 1−3	125.8	131.8	129.8	129.4	128.6	127.8	127.3	126.5	—
3 1 3	125.1	130.6	128.8	128.5	127.8	126.9	126.4	125.6	—
3 3−1	—	129.1	127.6	—	—	—	—	—	—
3 3 1	—	128.9	127.3	—	—	125.3	125.2	—	—
1 3−3	123.4	128.4	127.1	—	126.2	125.0	124.9	—	—
1 3 3	123.2	127.9	126.7	—	126.2	124.7	124.6	123.5	123.0

Note. Indexing refers to subcell only (true cells unknown, weak reflections omitted). —, Unobserved.

shows *Ln*: Te ratios between 1.5 and about 1.0 (see Table 3). The Dy and Ho compounds were identified also, but the samples always contained minor proportions of the tellurates (VI) Ln_6TeO_{12} (*12*), which, by large loss of TeO_2 and Te, under the same conditions were the only products from mixtures with Er, Tm, Yb, and Lu oxides.

The second series (*Ln* = La–Gd, Ce missing, Pm not investigated) shows higher *Ln*: Te ratios (1.6–2.2, see Table 3).

The X-ray powder diagrams of both series display groups of stronger reflections close to the Bragg angles of the corresponding cubic phases (*2*). They can be indexed by assuming monoclinic (or partly pseudotetragonal) deformations of the cubic fluorite cell (Tables 1 and 2). For lattice parameters see Table 3. They refer to unreduced subcells which correspond to the cell of fluorite. The standard deviations of the "monoclinic I" lattice constants are less than 0.6 pm (*a, b, c*) and 0.04° (β), and those of the "monoclinic II" and "pseudotetragonal" lattice constants are less than 1.0 pm and 0.06°, except for the Sm phase, where due to overlap a few reflections only could be used in calculating lattice constants. In this case the standard deviations are about one-half larger than above.

Highly sensitive X-ray records revealed, in addition to the indexed reflections, char-

TABLE II

OBSERVED *d* VALUES OF SECOND SERIES OF LOWER SYMMETRICAL ANTI-GLASS-RELATED PHASES ("MONOCLINIC II" AND "PSEUDOTETRAGONAL")

h k l	La	Pr	Nd	Sm	Eu(*t*)	Gd(*t*)
1 1−1	333.9	325.1	325.1	319.8	321.3	318.3
1 1 1	332.7	322.7	322.8	317.6	*	*
0 2 0	291.0	—	283.2	278.5	279.7	277.4
2 0 0	291.0	282.2	—	278.5	*	*
0 0 2	285.5	278.9	278.1	274.7	277.0	275.2
2 2 0	205.3	199.9	199.3	195.9	196.4	195.1
2 0−2	203.6	198.7	198.6	195.9	195.1	194.2
0 2 2	203.6	198.7	198.6	195.9	*	*
2 0 2	202.4	197.1	196.8	193.5	*	*
1 3−1	174.9	170.7	170.2	167.9	167.9	166.9
3 1−1	174.9	170.2	170.2	167.9	*	*
1 3 1	174.9	170.7	170.2	167.9	*	*
3 1 1	—	169.3	168.9	166.6	*	*
1 1−3	173.0	169.3	168.9	165.9	166.5	165.9
1 1 3	172.2	167.7	167.7	—	*	*
2 2−2	167.3	163.1	162.8	160.3	159.9	159.0
2 2 2	166.1	161.8	161.4	159.1	*	*
0 4 0	145.3	141.9	141.5	139.6	139.5	138.7
4 0 0	145.3	—	—	—	*	*
0 0 4	—	—	—	—	137.7	—
3 3−1	—	129.8	129.5	127.5	127.1	126.6
3 3 1	132.9	129.5	129.0	127.5	*	*
3 1−3	132.9	129.5	129.0	127.1	126.7	*
1 3−3	—	129.5	129.0	127.1	*	*
1 3 3	—	—	—	—	*	*
3 1 3	—	—	127.7	—	*	*

Note. Indexing refers to subcell only (true cells unknown, weak reflections omitted). —, Unobserved; *, reflection not separated from foregoing one in the case of pseudotetragonal indexing (*t*).

acteristic patterns of weak reflections which indicate much larger supercells for all samples. Figure 1 shows for the La and Eu phases of the first series shifts of reflections and some changes in intensity as expected when La is replaced by Eu in an isostructural phase. In the second series, the "pseudotetragonal" and "monoclinic II" La and Sm samples of different composition represent the same phase for each element and show almost identical patterns of weak reflections, except for minor shifts (for the La phase see Fig. 2). The weak reflections give no indications of "monoclinic I" phase being present in "monoclinic II" samples or vice versa.

We have not yet been able to index the weak reflections. Lattice constants and symmetry of the superstructures remain unknown, therefore, and the Debye–Waller parameters cannot be calculated. Luminescence, however, yields some evidence on anti-glass disorder.

B. Luminescence Properties

From the samples prepared those with the highest luminescence efficiency were selected for measurement of their luminescence properties. They are given in Table 4. The Eu^{3+} tellurites give a red luminescence. The spectra show the characteristic Eu^{3+} lines. The La^{3+} and Gd^{3+} tellurites give band emission and excitation spectra. These are due to transitions on the Te^{4+} ion, as discussed before (*3*). Since spectra of that kind were presented in Ref. (*3*), we

TABLE III

APPROXIMATE COMPOSITIONS, TEMPERATURE OF FORMATION, AND LATTICE CONSTANTS (SUBCELLS) OF LOWER SYMMETRICAL LANTHANOID TELLURITE PHASES

	Ln:Te	Te(VI) (wt. %)	*T* (°C)	*a* (pm)	*b* (pm)	*c* (pm)	*β* (°)
			"Monoclinic I" phases				
Y	1.02	0.70	810	552.6	530.0	543.9	90.28
La	1.26	0.61	1050	577.2	547.6	569.5	90.49
Pr	1.17	2.15	920	568.3	543.3	561.4	90.39
Nd	1.50	0.61	920	567.4	541.0	559.2	90.47
Sm	1.18	0.69	920	563.3	541.7	556.7	90.35
Eu	1.10	0.62	920	559.5	534.4	551.9	90.41
Gd	1.04	0.73	920	557.2	535.3	550.7	90.48
Dy	No pure phase		920	553.5	530.7	546.6	90.45
Ho	No pure phase		920	552.0	529.4	544.0	90.34
			"Monoclinic II" and "pseudotetragonal" (*t*) phases				
La	2.07	0.82	1050	580.2	581.6	570.8	90.55
La (*t*)	1.70	0.47	1050	579.2	—	563.5	—
Pr	1.73	2.79	915	563.5	567.6	556.7	90.61
Nd	1.62	0.60	915	562.0	566.0	556.7	90.68
Sm	2.21	0.22	1050	554	558	547	90.7
Sm (*t*)	1.90	0.44	1050	557	—	549	—
Eu (*t*)	1.77	0.44	1050	556.5	—	549.3	—
Gd (*t*)	1.79	2.50	1050	553.5	—	548.9	—

Note. Te(VI) contents refer to the overall weight of the samples.

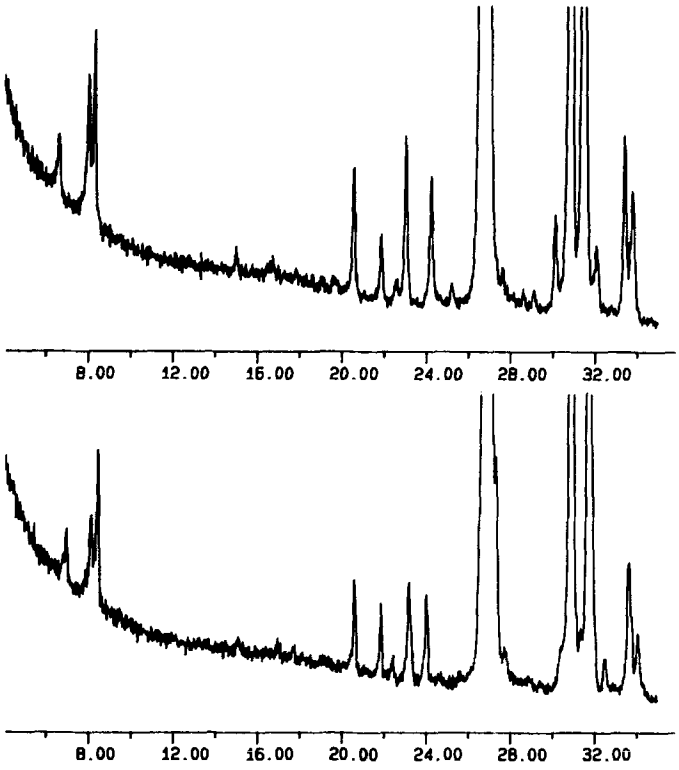

FIG. 1. Characteristic weak X-ray reflections indicating superstructure of "monoclinic I" La and Eu phases (2θ scale in degrees).

TABLE IV

SURVEY OF LUMINESCENT PROPERTIES AT 4.2 K OF SEVERAL LANTHANOID TELLURITE PHASES

	Main center			Additional center			
Ln	Emission max. (nm)	Excitation max. (nm)	$T_{1/2}$[a] (K)	Emission max. (nm)	Excitation max. (nm)	Nonlum. centers[b]	q[c]
			"Monoclinic I" phases				
La	540	290	110	–	–	+	Medium
Gd	530	285	80	490	320	+	Medium
Eu	Eu^{3+}	Eu^{3+}	30	–	– +	Medium	
			"Monoclinic II" and "pseudotetragonal" (t) phases				
La	470 ± 10[d]	310	100	–	–	–	High
La (t)	480	320	100	530	280, 330	+	Low
Gd (t)	480	320	100	530	290, 340	+	Low
Eu (t)	Eu^{3+}	Eu^{3+}	150	–	–	+	Medium

[a] Temperature at which the 4.2 K emission intensity has dropped 50%.
[b] From reflectance spectra. –, Absent; +, present.
[c] Estimated values of the quantum efficiency.
[d] Dependent on excitation wavelength.

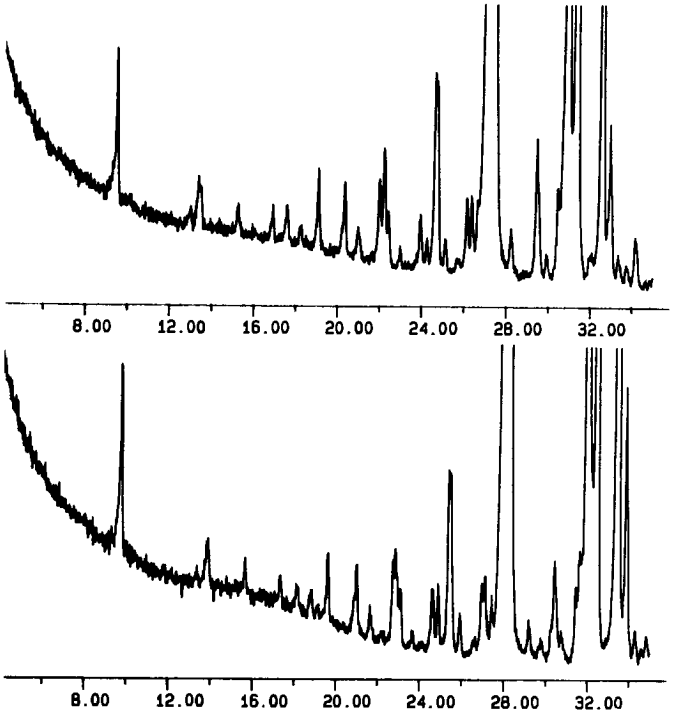

FIG. 2. Characteristic weak X-ray reflections indicating identical superstructure of "monoclinic II" and "pseudotetragonal" La phases.

give here only the maxima of the bands in the spectra. These are tabulated in Table 4. We have also included the values of $T_{1/2}$ which give some idea about the temperature quenching, estimates of the quantum efficiencies q, and information on the presence of nonluminescent centers. The latter was obtained from a comparison between the excitation and the diffuse reflectance spectra. When these spectra coincide, the number of quenching sites is low (i.e., $\ll 1\%$); when they do not, there is a certain concentration of quenching sites present ($>1\%$). As Table 4 shows, the reflectance spectra all show a tail into the longer wavelength region, with the exception of the "monoclinic II" La phase.

Let us start our discussion with the "monoclinic I" samples. The La phase is simple, because there is one emission band. Their maxima do not vary if the excitation wavelength or the emission wavelength is varied. This suggests strongly that we are dealing with one type of luminescent Te^{4+} ions. This situation is comparable to, for example, the luminescence of Cs_2TeBr_6 (*13, 14*), $Gd_3Sb_5O_{12}$ (*15*), and $Cs_2NaSbCl_6$ (*16*).

The fact that the quantum efficiency is medium is ascribed to the presence of nonluminescent centers. The emission band overlaps the absorption tail, so that energy transfer to the quenching sites is possible. The nature of these sites is not clear, but is most probably connected with deviations from stoichiometry. The temperature quenching is ascribed to quenching within the Te^{4+} centers.

The situation in the 'monoclinic I" Gd^{3+} tellurite is similar, but an additional (weaker) center appears which complicates the situation. By far the most information is

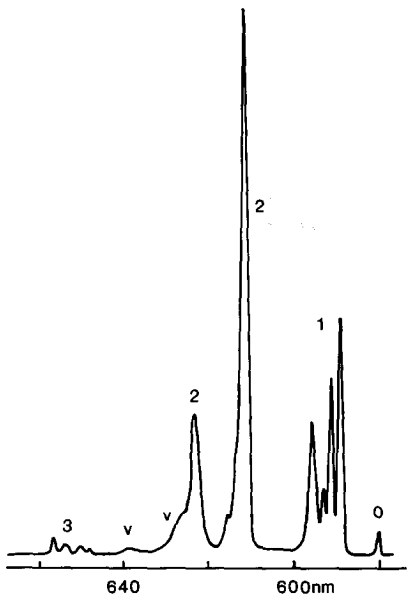

FIG. 3. Emission spectrum of "monoclinic I" Eu^{3+} tellurite at 4.2 K. Excitation into the $^5D_2$ level. The numbers indicate J in the transitions $^5D_0$–^7F_J. The v indicates the vibronic transitions.

given by the spectra of the corresponding Eu^{3+} tellurite. Figures 3 and 4 give some details. What is of importance here is the occurrence of sharp Eu^{3+} lines. The line width is 1–2 nm which is a typical value observed with completely ordered systems under the experimental conditions (*17, 18*). This fact proves that the structure is definitely not disordered.

In Fig. 3 the number of Eu^{3+} emission lines is as follows: $^5D_0$–$^7F_0$ 1 (1), $^5D_0$–$^7F_1$ 4–5 (3), $^5D_0$–$^7F_2$ 3–4 (5). The numbers in parentheses indicate the highest possible value if only one type of Eu^{3+} ions is present. The results show that there are probably two different Eu^{3+} ions present. The sharpness of the lines shows that the crystal field does not vary from site to site; i.e., the compound is ordered with probably two crystallographic sites for Eu^{3+}.

The Eu^{3+} spectra show some interesting details which will be discussed below. First we turn to the "monoclinic II" and "pseudotetragonal" phases. The "monoclinic II" La sample presents the most simple results (Table 4). There is one emission and one excitation band, no quenching centers, and the quantum efficiency is high. The emission maximum varies with excitation wavelength which indicates that we are dealing with one type of Te^{4+} center with varying crystal field, i.e., with varying coordination. Actually this luminescence is very similar to the one described for the Te-richer cubic anti-glass phase (*3*). This shows that the "monoclinic II" phase is disordered.

It is interesting to note that the ordered "monoclinic I" phase shows a considerably larger Stokes shift of the emission than the "monoclinic II" phase, viz., 16.500 cm^{-1} vs 11.500 cm^{-1}. We have recently shown that a larger Stokes shift for the Te^{4+} emission points to a stronger offset position in the ground state (*19*), i.e., a position with short distances to the ligands on one side and long ones on the other side. Using this

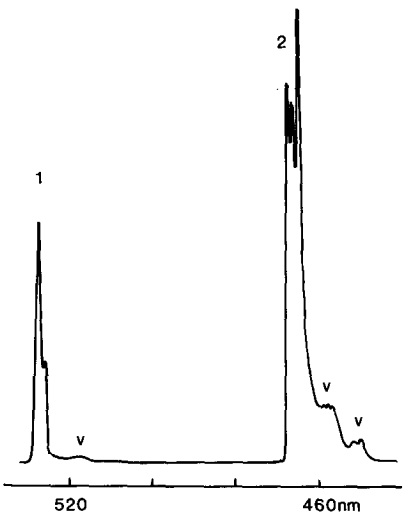

FIG. 4. Excitation spectrum of the Eu^{3+} emission of "monoclinic I" Eu^{3+} tellurite at 4.2 K. The emission wavelength is 612 nm. The numbers indicate J in the transitions $^7F_0$–^5D_J, whereas v indicates the vibronic lines.

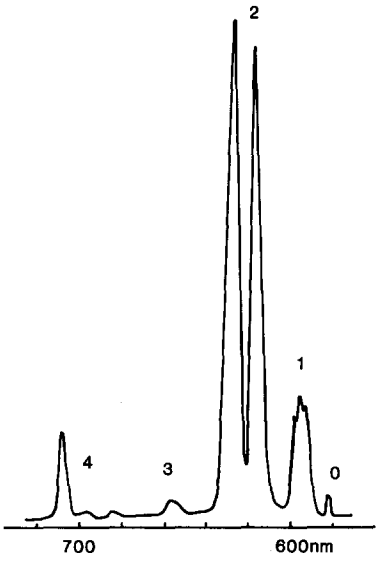

FIG. 5. Emission spectrum of "pseudotetragonal" Eu^{3+} tellurite at 4.2 K. See further Fig. 3. The difference in line width between Figs. 3 and 5 is roughly a factor 5.

relation, the ordered phase places Te^{4+} more offset than the disordered. It may be that in the ordered modification these offsets will also be ordered; i.e., they will enhance each other (cooperative effect).

In the "pseudotetragonal" phase the situation becomes complicated. The main emission is still that of the "monoclinic II" phase, but other centers are present as well, viz., quenching centers and a center with another luminescence characteristic. The Eu^{3+} phase, on the other hand, gives results which are easy to interpret: the emission spectrum consists of broad lines which can hardly be resolved (Fig. 5). The width of the emission lines is some 7 nm, i.e., about a factor of five larger than for the ordered "monoclinic I" phase. This large broadening indicates that the crystal field on the Eu^{3+} ion varies considerably from site to site; i.e., the direct surroundings of the Eu^{3+} ion differ from site to site. As a matter of fact the $^5D_0$–$^7F_0$ transition at about 580 nm is not so strongly broadened, because the levels involved are not degenerate so that the crystal field has no influence on these levels. Its width is nevertheless 2 nm which is a factor of three broader than for Eu^{3+} in the ordered monoclinic I phase. The Eu^{3+} emission yields the most convincing evidence that short-range order is highly disturbed in the "pseudotetragonal" phase.

In conclusion the luminescence properties of the lanthanoid tellurite phases described in this paper make it possible to decide on the degree of order. Since these luminescent properties are determined by short-range, and not by long-range order, the method is rather general, especially when the Eu^{3+} ion can be used.

Anti-glass disorder can be ruled out definitively for the "monoclinic I" phases, despite a statistical distribution of *Ln* and Te in equivalent positions (see above), and also despite their similarity to the cubic or "monoclinic II" anti-glass phases. The statement that of the phases investigated here only the "monoclinic II" or "pseudotetragonal" phases show anti-glass disorder is in full agreement with an investigation by Raman spectra (*10*).

Appendix: Spectroscopic Details in the Eu^{3+} Luminescence

In this section we pay attention to some interesting details in the Eu^{3+} luminescence. First we note that the excitation spectra of the Eu^{3+} emission contain a broadband which coincides with the Te^{4+} absorption of the corresponding La^{3+} and Gd^{3+} sample. This indicates energy transfer from Te^{4+} to Eu^{3+} (see also Ref. (*3*)). The Eu^{3+} charge transfer band cannot be observed; it is hidden under the $^1S_0 \rightarrow {}^3P_1$ absorption band of the Te^{4+} ion.

Second we note a striking difference between the values of $T_{1/2}$ for both Eu^{3+} phases (see Table 4). These values were determined for $^5D_2$ excitation. Nonradiative

TABLE V

COOPERATIVE VIBRONIC LINES IN THE SPECTRA AT 4.2 K OF Eu^{3+} TELLURITES (VALUES IN cm^{-1})

	"Monoclinic I", excitation	
21.410	$^7F_0$–$^5D_2$	
21.790	$^7F_0$–$^5D_2$ + 380	Te–O def.
22.160	$^7F_0$–$^5D_2$ + 750	Te–O stretch
18.975	$^7F_0$–$^5D_1$	
~19.320	$^7F_0$–$^5D_1$ + ~345	Te–O def.
	"Monoclinic I", emission	
16.340	$^5D_0$–$^7F_2$ (a)	
16.040	$^5D_0$–$^7F_2$ (b)	
15.950	$^5D_0$–$^7F_2$ (a) − 390	Te–O def.
15.650	$^5D_0$–$^7F_2$ (b) − 390	Te–O def.
	"Pseudotetragonal", excitation	
21.410	$^7F_0$–$^5D_2$	
21.760	$^7F_0$–$^5D_2$ + 350	Te–O def.
22.140	$^7F_0$–$^5D_2$ + 730	Te–O stretch
18.960	$^7F_0$–$^5D_1$	
19.300	$^7F_0$–$^5D_1$ + 340	Te–O def.
17.230	$^7F_0$–$^5D_0$	
17.570	$^7F_0$–$^5D_0$ + 340	Te–O def.
~17.985	$^7F_0$–$^5D_0$ + ~755	Te–O stretch

transitions from this or lower levels are hard to imagine. The quenching is, therefore, ascribed to energy migration over the Eu^{3+} ions to quenching sites (*4, 20*). This migration is thermally activated (*21*). It is interesting to note that the ordered phase has a much lower $T_{1/2}$, i.e., a lower activation energy than the disordered one. This corroborates our conclusion: in the disordered phase the crystal field on the Eu^{3+} ion varies from site to site: i.e., the energy levels vary also from site to site, so that the energy mismatches will be much larger than in the ordered phase The mismatches are the energy differences which determine the thermal activation. Finally we draw attention to the cooperative vibronic lines (*22*) in the spectra. These are due to transitions in which an electronic transition on the Eu^{3+} ion is coupled with a vibrational transition on the neighboring tellurite group. Figures 3–5 show some of these, whereas Table 5 gives a survey and an assignment. There is a coupling with the Te–O deformational mode and with the Te–O stretching mode. The former is the stronger, which is quite exceptional. We have recently observed similar transitions for Eu^{3+} in Eu^{3+} nitrates (*18, 23*).

Acknowledgments

This investigation was supported by the Deutsche Forschungsgemeinschaft and by the Fonds der Chemischen Industrie. Mr. H. Jepsen, Fachbereich Geowissenschaften der Universität, Marburg, FRG, recorded the X-ray diffraction diagrams with the Siemens D 500 powder diffractometer. Calculations were done at the Hochschulrechenzentrum Frankfurt.

References

1. H.-G. BURCKHARDT AND M. TRÖMEL, *Acta Crystallogr. Sect. C* **39,** 1322 (1983).
2. M. TRÖMEL, W. HÜTZLER, AND E. MÜNCH, *J. Less-Common Met.* **110,** 421 (1985).
3. G. BLASSE, G. J. DIRKSEN, E. W. J. L. OOMEN, AND M. TRÖMEL, *J. Solid State Chem.* **63,** 148 (1986).
4. G. BLASSE, *Mater. Chem. Phys.* **16,** 201 (1987); G. BLASSE, *Prog. Solid State Chem.* **18,** 79 (1988).
5. RANFAGNI, D. MUGNAI, M. BACCI, G. VILIANI, AND M. P. FONTANA, *Adv. Phys.* **32,** 823 (1983).
6. M. WEBER, *Ioniz. Radiat.* **14,** 3 (1987).
7. M. TRÖMEL, *J. Solid State Chem.* **35,** 90 (1980).
8. M. TRÖMEL, E. MÜNCH, AND L. MARTIN, *Z. Kristallogr.* **174,** 197 (1986).
9. G. BLASSE, *in* "Handbook on the Physics and Chemistry of the Rare Earths" (K. Gschneidner, Jr., and L. Eyring, Eds.), Chap. 34, North-Holland, Amsterdam, 1979.
10. E.-J. ZEHNDER, L. MARTIN, E. MÜNCH, AND M. TRÖMEL, unpublished; see also M. TRÖMEL, *Z. Kristallogr.*, in press.
11. M. J. REDMAN, W. P. BINNIE, AND J. R. CARTER, *J. Less-Common Met.* **16,** 407 (1968).
12. G. BLASSE, *J. Inorg. Nucl. Chem.* **31,** 3335 (1969).
13. R. WERNICKE, H. KUPKA, W. ENSSLIN, AND H. H. SCHMIDTKE, *Chem. Phys.* **47,** 235 (1980).
14. G. BLASSE, G. J. DIRKSEN, AND P. A. M. BERDOWSKI, *Chem. Phys. Lett.* **112,** 313 (1984).
15. G. BLASSE AND H. S. KILIAAN, *Inorg. Chim. Acta* **117,** L 23 (1986).
16. E. W. J. L. OOMEN, W. M. A. SMIT, AND G. BLASSE, *Chem. Phys. Lett.* **138,** 23 (1987).

17. H. S. KILIAAN, J. F. A. K. KOTTE, AND G. BLASSE, *Chem. Phys. Lett.* **133,** 425 (1987).
18. G. BLASSE, G. J. DIRKSEN, AND J. P. M. VAN VLIET, *Inorg. Chim. Acta* **142,** 165 (1988).
19. G. BLASSE, G. J. DIRKSEN, AND W. ABRIEL, *Chem. Phys. Lett.* **136,** 460 (1987).
20. G. BLASSE, *Recl. Trav. Chim. Pays-Bas* **105,** 143 (1986).
21. M. BUIJS AND G. BLASSE, *J. Luminesc.* **34,** 263 (1986).
22. M. STAVOLA, L. ISGANITIS, AND M. G. SCEATS, *J. Chem. Phys.* **74,** 4228 (1981).
23. G. BLASSE, G. J. DIRKSEN, AND J. P. M. VAN VLIET, *Recl. Trav. Chim. Pays-Bas* **107,** 138 (1988).